Determination of the oxidation state by resonant-Raman scattering spectroscopy

Juan José Leani,*[a] Héctor Jorge Sánchez,[ac] María Valentinuzzi[ac] and Carlos Pérez[b]

Received 15th June 2010, Accepted 21st October 2010
DOI: 10.1039/c0ja00046a

X-Ray fluorescence spectra present singular characteristics produced by the different scattering processes. When atoms are irradiated with incident energy lower and close to an absorption edge, scattering peaks appear due to an inelastic process known as resonant Raman scattering (RRS). In this process, the emitted photons have a continuous energy distribution with a high energy cut-off limit. This work presents results regarding the possibility of determining the oxidation state by resonant Raman scattering using an energy dispersive system. Pure samples of transition metals (Cu, Fe, Mn) and different oxides of them (CuO, Cu_2O, Fe_2O_3, Mn_2O_3, MnO_2) were irradiated with monochromatic synchrotron radiation below their absorption edges to inspect the RRS emissions. The spectra were analyzed with specific programs using non-conventional functions for data fitting and a FFT smoothing procedure was applied. After smoothing, the RRS residuals are studied in order to detect variation with respect to the theoretical curve. These variations are closely related with the chemical environments of the absorbing element and can provide relevant structural information of the sample. The changes existing in the RRS structure between pure elements and their oxides are clearly discriminated and suggest the possibility of structural characterization by means of resonant Raman scattering using an energy-dispersive system combined with synchrotron radiation.

I. Introduction

When atoms are irradiated by X-ray photons different kinds of interactions take place: the photon can be absorbed by the photoelectric effect or can suffer a Rayleigh or Compton scattering. However, under resonant conditions, other low probability interactions can occur. One of these interactions is the resonant Raman scattering (RRS).[1]

The X-ray resonant Raman scattering is an inelastic scattering process which presents fundamental differences compared to other scattering interactions between X-rays and atoms; when the energy of the incident photon approaches from below to the absorption edge of the target element, a strong resonant behavior takes place contributing to the attenuation of X-rays in matter. According to the absorption–emission model the RRS process can be represented by three steps:[2]

(1) The initial state consists of an incident photon with an energy below to the K (or L3, L2,…) threshold.

(2) A hole is produced in the K (or L3, L2,…) shell and the excited electron is ejected to an unoccupied state; an electron from a higher shell fills the vacancy and a photon is emitted.

(3) The final state consists of a hole in the higher shell, a scattered photon and an excited electron (in the continuum or in an excited bound state).

Fig. 1 represents the scattering process when the incident photon has energy below to the K absorption edge and the K hole is filled by an electron from the L shell. This is the KL-type scattering. The incident photon has an energy E_i lower than the energy of the K threshold; the energy of the incident photon is absorbed by a K shell electron producing a hole and an electron in the continuum with kinetic energy k. The K shell vacancy is filled by an electron from the L shell (being Ω_L the energy of the L threshold) and a photon is emitted with energy E_S.

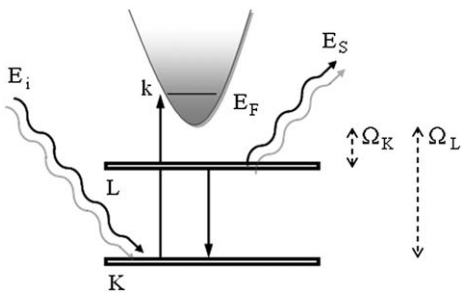

Fig. 1 Schematic representation of a KL resonant Raman scattering process.

Assuming a well defined energy of the incident photon, the energy conservation for the scattering process leads to:[3]

$$E_i - \Omega_L - E_F = E_S + \kappa \quad (1)$$

where E_F is the Fermi energy. This equation indicates that between initial and final states the available energy has to be shared between the outgoing electron and the emitted photon.

The resonant nature of the process and the existence of an onset energy in RRS spectrum enable the probing of the edge structure characteristics by tunning the incident energy towards the edge. In the case of oxide compounds, the Raman peak changes the maximum energy, corresponding to an excited

[a]*Facultad de Matemática Astronomía y Física, Universidad Nacional de Córdoba, 5000 Córdoba, Argentina. E-mail: lj@famaf.unc.edu.ar*
[b]*Laboratorio Nacional de Luz Síncrotron, CP 6192/CEP 13084-971 Campinas, Brazil*
[c]*CONICET, Argentina*

electron with kinetic energy equal to zero; the Raman peak shifts to energies lower by a few electron volts due to the change of the absorption edge energy.[4] In the last few years, experiments of resonant X-ray scattering and inelastic resonant scattering have become a powerful technique to investigate electronic states in solids.[5,6]

By analysing the spectrum pattern present in the low-energy tail of the Raman peak, the oxidation state of an element can be determined. This behaviour could be used for laying the foundations of a new spectroscopy technique for structural characterization. Such a technique would offer complementary information to that obtained by other established techniques, such as a XANES, EXAFS, XRD, *etc*.

The spectra were analyzed with specific programs for fitting theoretical expressions to the experimental data. After that residuals were determined in the low energy side of the RRS peaks and a FFT smoothing procedure, taking into account the instrument functions of the detecting system, was applied. Then the experimental RRS residuals were studied in order to detect variation with the theoretical curve. Employing a low resolution detecting system, changes in the RRS structure can be observed, providing the possibility to identify the elements of a sample and their oxidation state.[7,8] This is an important fact since the chemical environment of an absorbing element affects the emission of its characteristic X-rays; the formation of chemical bonding causes a migration of the valence electrons among participant atoms, reducing screening effects and increasing their inner shell binding energies.

II. Measurements and data analysis

The measurements were carried out in XRF station of the D09B-XRF beamline[9] at the Brazilian synchrotron facility (LNLS, Campinas).[10] This synchrotron light source operates at a nominal energy of 1.37 GeV with a maximum current of 250 mA in multibunch mode, emitting photons with a critical energy of 2.08 keV. The XRF beamline is equipped with a double crystal "channel-cut" monochromator, the energy resolution of the monochromator is $\cong 3$ eV at 10 keV using a Si(111) crystal. For the measurements performed in this work, the incident beam was collimated with orthogonal slits to 1×1 mm and monitored with ionisation chambers, resulting in a flux intensity on the sample of $\cong 10^8$ ph s^{-1} @ 10 keV. The detection systems are energy-dispersive setups composed by several solid-state detectors with different windows and different electronic chains. The detector used in this work was an Ultra-LEGe solid-state detector with a Be windows of 8 μm and an energy resolution of 158 eV for the Mn Kα line. Pulse processing was accomplished by a fast amplifier with triangular shaping and spectra were processed and collected with a 8K MCA. The experimental geometry was the typical 45° + 45° configuration on the electron orbit plane to reduce Compton and Rayleigh scattering; the measurements were carried out in air atmosphere, taking into account the air absorption.

Although the exact value of the absorption edge energy is not imposing for the subsequent calculations, a precise knowledge of the edge energy is needed to assure that the energy of the incident photons is below the absorption edge, *i.e.*, photoelectric effects is not produced. With this aim, a further scanning in every sample was performed in order to determine the edge energy. It was attained by scanning 40 eV in steps of 1 eV around the absorption edge with a measuring lifetime of 5 s.

In the case of Cu, the samples consisted of pure foils (>99.9%) with a thickness of 7.5 μm and compacted powder of oxide standards (>99%) of CuO and Cu_2O with a thickness of 5 mm. These samples were irradiated with monochromatic photons of 8915 eV, *i.e.*, below the K-edge of the element of interest to inspect the Raman emissions. The measuring lifetime was 1500 s.

In the case of Fe and Mn, samples consisted of pure foils (>99.9%) with a thickness of 7.5 μm and compacted powder of oxide standards (>99%) of Fe_2O_3, Mn_2O_3 and MnO_2 with a thickness of around 5 mm. The Fe and Mn samples were irradiated with monochromatic photons of 7022 eV and 6450 eV respectively. The measuring lifetime was 3500 s for Fe and 6500 s for Mn. For a comparison, the obtained Raman spectra for the Mn samples are shown in Fig. 2.

Spectra were analysed with specific programs for spectrum analysis (Peakfit,[11] TableCurve[12]) using non-conventional functions for data fitting, *i.e.*, modified Voight functions (for Compton peaks), Gaussian functions for fluorescent and for low intensity peaks (such as escape peaks and other contributions), and polynomial functions for the background.

Raman peaks were fitted using specific functions:[2,4]

$$Y(E_S) = \Phi \int_0^{E_i - \Omega_L - E_F} \frac{E}{(\Omega_K - \Omega_L - E)^2} e^{\frac{(E_S - E)^2}{2\delta^2}} dE \qquad (2)$$

where E_i is the incident energy, E_S is the scattered energy, the Gaussian term stands for the instrumental function, the factor δ represents the detector resolution and Φ is a constant factor that stands for the incident intensity, solid angles, detector efficiency, *etc*.

The data fitting using this theoretical expression was acceptable in the low energy region but the model did not reproduce with precision the spectrum behaviour in the region near to the Raman peak centre. It was observed that a more precise data fitting of the low energy side of Raman peaks was attained by using a Lorentzian expression:

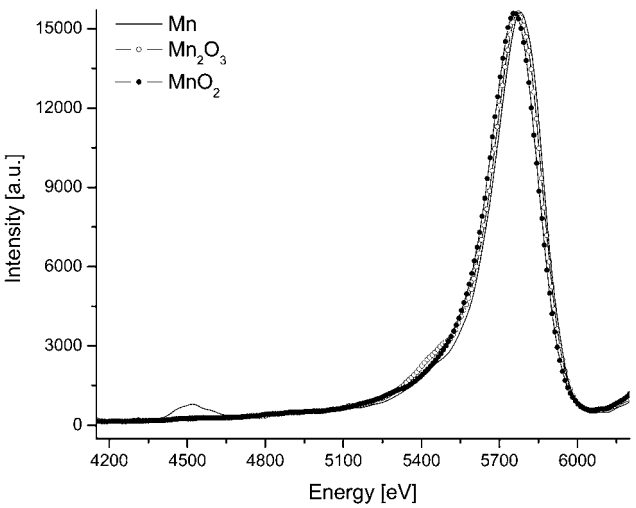

Fig. 2 KL-RRS spectra obtained for Mn, Mn_2O_3 and MnO_2 samples with incident energy of 6450 eV.

$$y = y_0 + \frac{2A}{\pi}\frac{\omega}{4(x-x_0)^2+\omega^2} \quad (3)$$

where y_0 is the baseline offset; A is the area under the curve from the baseline; x_0 is the center of the peak and ω is the full width of the peak at half height. Note that the parameters in the Lorentzian model (eqn (3)) are similar to the parameters defined for the Gaussian model used in the Raman expression (eqn (2)); therefore, both fits are very similar, as expected. The Lorentzian expression was selected by the used software[12] among almost 3000 possible theoretical expressions for fitting of the data, possibly because it fits with high accuracy ($r^2 > 0.999$) also the low energy tail of the inelastic peaks. This high level of precision is crucial in order to be certain that residuals between theoretical model and the experimental spectrum provide physical information and not be originated by an incorrect fitting. The low energy side of Raman peaks (starting just in the peak center) fitted using Lorentzian peaks can be appreciated in Fig. 3.

In the experimental spectra, after the theoretical fitting, a FFT smooth procedure was applied. In general, experimental data are often contaminated by noise originated mainly from the experiment itself and also by noise related to the measurement process. In this work, a standard denoising method was employed based on the frequency decomposition of the signal.[13] A FFT smoothing procedure was applied considering a Gaussian instrumental-function with a σ of 67 eV. The smoothing is accomplished by removing Fourier components with frequencies larger than $(1/n\Delta t)$ where n is the number of data points considered at a time and Δt is the time spacing between two adjacent data points. The function used to clip out the high frequency components is a parabola with its maximum of one at zero frequency and falling to zero at the cut-off frequency. The parameters of this parabolic clipping function are determined by the total number of points and the number of points considered at one time; the more points considered at one time, the greater the degree of the smoothing. By suppressing the high frequency components, the noise associated with them can be eliminated. It works as a perfect low-pass filter where the cut-off frequency plays the role of a parameter during the analysis.

This kind of filter offers a very important physical sense at the moment of inspecting the experimental data, in opposition to the methods that are purely mathematics (for example, methods based in pondered averages).

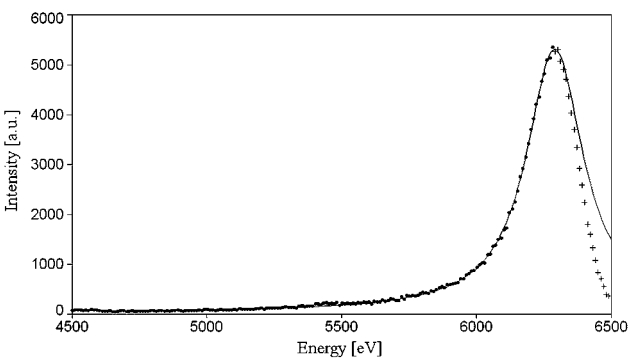

Fig. 3 KL-RRS spectrum obtained for a Fe sample with incident energy of 7022 eV. Solid line represents data fitting using eqn (3).

It should be noted that the data analysis is relatively simple and direct, in comparison with the data treatment required for other techniques (*e.g.* EXAFS). This simplicity, in addition to the low number of steps to reach the final result, turns this analysis into a precise and reliable procedure. In addition, the errors are completely quantifiable since the statistical basis used are well known.

III. Results and discussions

As mentioned before, the first step of the analysis is to check the absorption edge energy of the target elements; this stage has the aim of establishing certainly whether the sample is excited under resonant or fluorescent conditions. This stage is attained by applying the well-known method of inspecting the derivate change of the emitted intensity on the edge rising vicinity. The obtained values were 8.978 ± 0.003 keV for Cu, 7.111 ± 0.003 keV for Fe and 6.539 ± 0.003 keV for Mn. The K-absorption edges of pure samples are in agreement with the tabulated of 8.979 keV for Cu, 7.112 keV for Fe and 6.539 keV for Mn.[14] In addition to this result, it was checked that the absorption edge energy increases with the oxidation state in all the samples, in agreement with the expected behaviour.

As it should be expected, the Raman scattering process is resonantly enhanced as the energy of the incident photons becomes closer to the K absorption threshold; in addition, the Raman peak is more intense, dominating over the Compton peak. This behavior was observed in all samples. In the case of oxides, the Raman peak changes the maximum energy (corresponding to an excited electron with kinetic energy equal to zero) according to eqn (1), as explained in Introduction. Each Raman peak shifts to lower energies a few electron volts due to the change of the absorption edge energy.

The low energy residuals (just below of Raman peaks center) between the theoretical expression and the measured spectra (after the smoothing procedure), are shown in Fig. 4, 5 and 6 for the Cu, Fe and Mn samples, respectively.

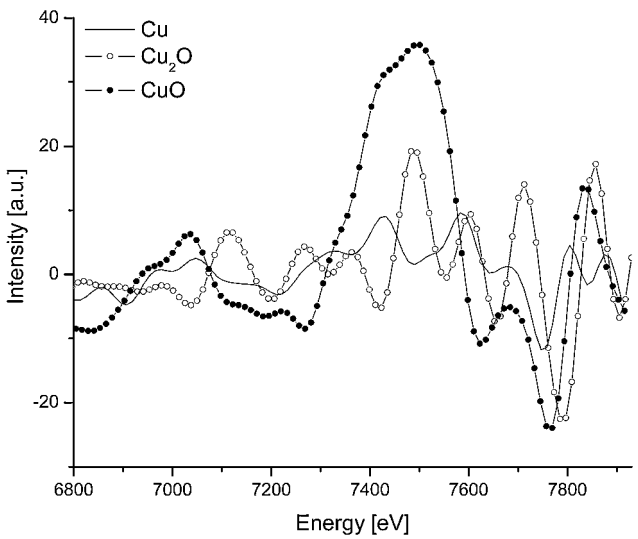

Fig. 4 Cu, Cu_2O and CuO residuals between the experimental Raman spectrum and the data fitting using eqn (3).

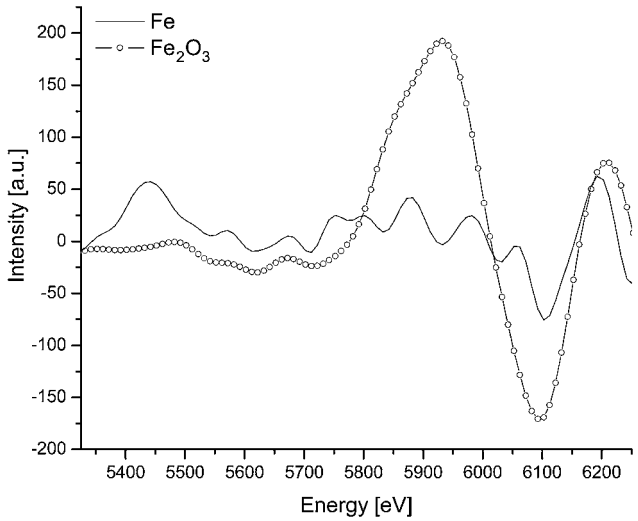

Fig. 5 Fe and Fe_2O_3 residuals between the experimental Raman spectrum and the data fitting using eqn (3).

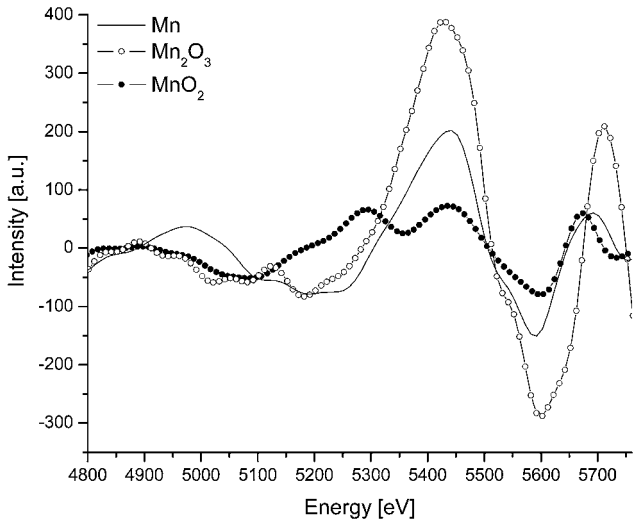

Fig. 6 Mn and Mn_2O_3 residuals between the experimental Raman spectrum and the data fitting using eqn (3).

The results in this work do not take into account infrared divergence or bremsstrahlung contributions to the background. In addition, its contribution is important mostly in low energy areas and does not affect significantly the range of the scattered line, *i.e.*, the range of interest of this work. Regarding the self-absorption effects, they were not taken into account. Certainly, these both effects would be considered in the calculations. However, both bremsstrahlung and self-absorption effects are smooth and continuous functions of the energy that do not interfere with the fast variations in the spectra that we are studying. Moreover, these effects have the same energy distribution in all the studied samples, being compensated in the spectral comparison.

As can be appreciated, the RRS residuals of oxides are quite different from the residuals of the pure elements, in the three groups of samples. In the case of the Cu_2O sample, we can see that the oscillations present in the RRS residuals are smooth, such as the ones that we found in the Cu RRS residuals. However, in some regions (see region close to 7490 eV and the region from 7640 eV to the end of the spectrum), there are oscillations quite similar to the ones presents in the CuO residuals. Therefore, this simple quantitative analysis based on the oscillation pattern present in the Cu_2O RRS residuals shows that this compound has an intermediate oxidation state between the other Cu studied samples. If we put now our attention in the Fe(III) and Mn(III) oxide residuals shown in Fig. 5 and 6 respectively, we can see that both residuals present the same oscillation patterns and relative intensities, mainly in the region close to the peak center. This behavior is expected since these oxides have the same oxidation state and they belong to transition metals of proximate atomic number. These results and their consideration also evidence that the oscillation pattern appearing in the residuals exposes physical processes and it is not a mere fitting artifact.

A general improvement of the theoretical models is clearly needed. A low order interactions, such as spin parity effects, molecular and atomic bounding vacancies, *etc.*, must be take into account in order to achieve a better fitting between the model and the experimental data, reaching in this way a deep physical understanding of the processes involved in this inelastic scattering procedure. To these improvements of the theoretical model is in part pointed our current investigation.

This work is pioneer in the area and an important work of interpretation is necessary in the future. Nevertheless, this behaviour in the residuals of compounds could be used to identify the oxidation state of the elements under study, offering a possibility of chemical environment determination using RRS spectroscopy.

IV. Conclusions

The results shown above point out the existence of a clear difference among the measured samples, *i.e.* the oxidation states of transition metals.

These results suggest the possibility of structural characterization by means of resonant Raman scattering using an energy-dispersive system combined with synchrotron radiation.

A RRS chemical environment technique would offer an opportunity to study the oxidation state of different kind of samples, such as mineral, environmental and/or biological samples, or samples in which a complete characterization is impossible to achieve by other methods, such as conventional absorption techniques.

Nowadays, it is too soon to speak about advantages or disadvantages of this new method. Nevertheless, possible advantageous applications or situations could be the possibility of using conventional XRF spectrometers to perform structural analysis by employing monochromators or secondary targets. In addition, portable XRF spectrometers with secondary target could be used to *in situ* oxides analysis of environmental, archeological or art samples.

Further investigations and measurements are currently carried out in order to reach a better understanding of the processes involved and the implementation of a practical procedure. Future perspectives include analysis of the oscillation patterns by means of Fast Fourier Transform (FFT) procedures in order to

study only characteristic frequencies, avoiding self-absorptions and other secondary effects.

Acknowledgements

This work was partially supported by the LNLS (Campinas, Brazil).

References

1 A. G. Karydas and T. Paradellis, *J. Phys. B: At., Mol. Opt. Phys.*, 1997, **30**, 1893.
2 H. J. Sánchez, M. C. Valentinuzzi and C. Pérez, *J. Phys. B: At., Mol. Opt. Phys.*, 2006, **39**, 1.
3 J. Rubensson, *J. Electron Spectrosc. Relat. Phenom.*, 2000, **135**, 110–111.
4 M. C. Valentinuzzi, H. J. Sanchez, J. Abraham and C. Perez, *X-Ray Spectrom.*, 2008, **37**, 555.
5 K. Ishii, K. Tsutsui, Y. Endoh, T. Tohyama, S. Maekawa, M. Hoesch, K. Kuzushita, M. Tsubota, T. Inami, J. Mizuki, Y. Murakami and K. Yamada, *Phys. Rev. Lett.*, 2005, **94**, 207003.
6 A. Kotani and S. Shin, *Rev. Mod. Phys.*, 2001, **73**, 203.
7 A. G. Karydas, S. Galanopoulos, T. ChZarkadasParadellis and N. Kallithrakas-Kontos, *J. Phys.: Condens. Matter*, 2002, **14**, 12367.
8 J. Szlachetko, C. L. Dousse, J. Hoszowska, M. Pajek, R. Barret, M. Berset, K. Fennane, A. Kubala-Kukus and M. Szlacheto, *Phys. Rev. Lett.*, 2006, **97**, 073001.
9 C. A. Pérez, M. Radke, H. J. Sánchez, H. Tolentino, R. T. Neuenshwander, W. Barg, M. Rubio, M. I. Silveira Bueno, I. M. Raimundo and J. R. Rohwedder, *X-Ray Spectrom.*, 1999, **28**, 320.
10 A. R. D. Rodrigues, R. H. A Farias, M. J. Ferreira, G. S. Franco, L. C. Janhnel, L. Lin, A. C. Lira, R. T. Neuneschwander, C. Pardine, F. Rafael, A. Rosa, C. Scorzato, C. E. T. Goncalves da Silva, A. Romeu da Silva, P. F. Tavares, D. Wisnivesky and A. Craievich, *Proceedings of the Particle Accelarator Conference—PAC97*, Vancouver, 1997.
11 PeakFit v4.12 for Windows, Copyright 2003, SeaSolve Software Inc., Portions Copyright 2000–2003 SYSTAT Software Inc.
12 TableCurve v1.11 for Windows. Copyright 1993, AISN Software.
13 Q. Zhang, R. Aliaga-Rossel and P. Choi, *Meas. Sci. Technol.*, 2006, **17**, 731.
14 J. A. Bearden and A. F. Burr, *Rev. Mod. Phys.*, 1967, **39**, 125.

